Nano Research 2014, 7(2): 228–235
DOI 10.1007/s12274-013-0390-y
Research Article
ISSN 1998-0124
CN 11-5974/O4

Structural and optical verification of residual strain effect in single crystalline CdTe nanowires

Liubing Huang[1], Siyuan Lu[2], Paichun Chang[1], Karan Banerjee[1], Robert Hellwarth[1], and Jia Grace Lu[1] (✉)

[1] *Department of Physics and Astronomy, Department of Electrical Engineering, University of Southern California, Los Angeles, CA90089, USA*
[2] *IBM Thomas J. Watson Research Center, 1101 Kitchawan Road, Yorktown Heights, NY 10598, USA*

Received: 16 August 2013
Revised: 15 November 2013
Accepted: 17 November 2013

© Tsinghua University Press and Springer-Verlag Berlin Heidelberg 2013

KEYWORDS

CdTe nanowire,
single crystalline,
chemical vapor deposition,
residual strain,
photoluminescence

ABSTRACT

Single crystalline CdTe nanowires have been synthesized using Au-catalyzed chemical vapor deposition. X-ray diffraction reveals the existence of non-negligible inhomogeneous compressive strain in the nanowires along the <111> growth direction. The effect of the strain on the electronic structure is manifested by the blue-shifted and broadened photoluminescence spectra involving shallow donor/acceptor states. Such residual strain is of great importance for a better understanding of the optical and electrical behaviors of various semiconductor nanomaterials as well as for device design and applications.

Cadmium telluride (CdTe) has attracted significant research interest because of its superior optical and electrical properties for developing optoelectronic devices. In particular, it holds promising potential for low-cost photovoltaics due to its high absorption coefficient, absorbing 99% of the incident light in a layer thickness of only ~1 μm, as compared to ~10 μm for Si. In addition, it has a direct band gap of 1.49 eV at room temperature, which is close to the theoretically-calculated optimal value for solar cells under AM 1.5 irradiation. Furthermore, the band gap of CdTe can be readily engineered by alloying with mercury or zinc, and thus it can function as an effective photo-detector with a wide spectral range. Moreover, CdTe nanowires with high aspect ratio are exceptional for building high performance photoelectric devices since they possess the unique properties of nanostructured systems.

Various techniques have been developed to synthesize CdTe nanowires including template-directed electrochemical deposition [1], catalytic solution growth [2], self-assembling nanoparticles into nanowires [3] and hydrothermal methods [4, 5]. However, most of these methods are solution-based, and the resulting nanowires are typically polycrystalline. Little has been done on synthesis of single crystalline CdTe nanowires [6, 7].

Address correspondence to jialu@usc.edu

Even with the chemical vapor deposition (CVD) method, which is known as an efficient way to synthesize single crystalline nanowires [8, 9], the growth mechanisms for CdTe nanowires are not yet clearly understood. Specifically, the effect of the ambient gas on the reaction mechanism has not been fully studied.

In this article, we first describe the Au-catalyzed CVD growth of single crystalline CdTe nanowires, followed by careful structural and optical characterization of the nanowires. Experimental evidence is used to elucidate the nanowire growth mechanism via a hydrogen-assisted vapor–solid–solid (VSS) process. Most significantly, we demonstrate the existence of non-negligible inhomogeneous residual strain in the as-synthesized CdTe nanowires, and the impact of such strain on the electronic structure of the nanowires manifested in their photoluminescence response. This study indicates that residual strain effect has to be taken into consideration for the sensible design and performance control of nanowire based devices. The details of nanowire growth and characterization results are discussed below.

The catalytic CVD growth of CdTe utilized a quartz tube furnace. An alumina boat with source CdTe powder (99.999%, from Alfa Aesar) was placed at the centre of the furnace. A Si wafer was etched in buffered oxide etch (BOE) solution to remove the native oxide layer followed by coating with 10 nm Au film as the catalyst. The Si substrate was placed at the furnace 10 cm away from the source powder. The system was pumped for 30 min to ~40 Pascal. The furnace temperature was set at 465 ℃, resulting in a source temperature of 465 ℃ and a substrate temperature of 350 ℃. The CdTe nanowires were grown for 1 h under continuous 10 standard cubic centimeters per minute (sccm) H_2 gas flow.

The morphology and composition of as-grown CdTe nanowires were characterized by field emission scanning electron microscopy (FESEM, Hitachi S4800), transmission electron microscopy (TEM, JEOL 2000), and energy dispersive X-ray fluorescence (EDS, fitted in the JEOL 2000 microscope). The structural properties were studied by powder X-ray diffraction (XRD, Rigaku Ultima IV diffractometer, Cu Kα, λ = 1.5418 Å, acceleration voltage V = 40 kV, emission current I = 20 mA) in $\theta/2\theta$ mode with a scan speed of 4°/min and Bragg angle 2θ ranging from 20° to 80°. All the peak parameters (peak position, full width at half maximum (FWHM) and the corresponding lattice constant) were identified by MDI Jade 5.0 software. The optical properties were studied by photoluminescence (PL) in the temperature range 5.0 to 79.7 K under CW green laser (532 nm, ~1.1 W/cm^2) excitation. The laser spot radius was ~200 μm and the PL spectra were taken from hundreds of nanowires.

Figure 1 shows a scanning electron microscope (SEM) image of the as-grown CdTe nanowires with diameters ranging from 50 to 200 nm and lengths from 5 to 20 μm. Polygonal nanoparticles are found on the tips of the nanowires, suggesting a catalytic growth mechanism. Figure 2(a) is a low magnification TEM image of a typical CdTe nanowire with smooth surfaces and uniform thickness along the nanowire axis. A polygonal nanoparticle was found on the tip of the nanowire, consistent with the SEM observation. Figure 2(b) shows a high resolution transmission electron microscope (HRTEM) images of a single CdTe nanowire in the zone axis $[0\bar{1}1]$. The interplanar distance is determined to be 0.37 nm, corresponding to the <111> direction in zinc blende CdTe. The insert displays a selected area electron diffraction (SAED) pattern of CdTe nanowires, verifying the single crystalline nature. The pattern can be indexed to the zinc blende structure CdTe with growth direction

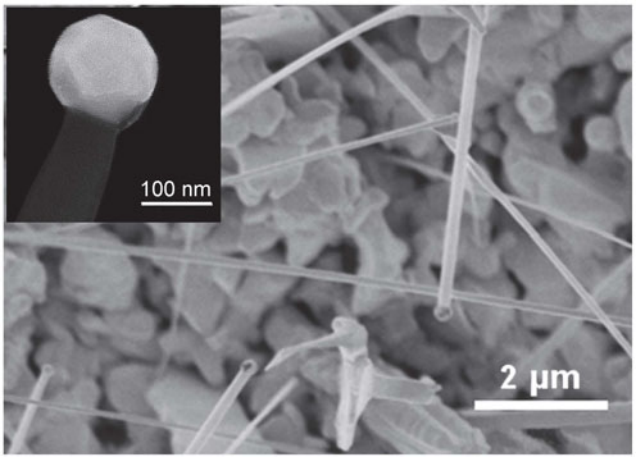

Figure 1 SEM image of as-grown CdTe nanowires; polygonal nanoparticles are found on the tips of the nanowires. Insert: High resolution SEM image of the Au catalyst shows a polygonal shape, verifying the VSS growth mechanism.

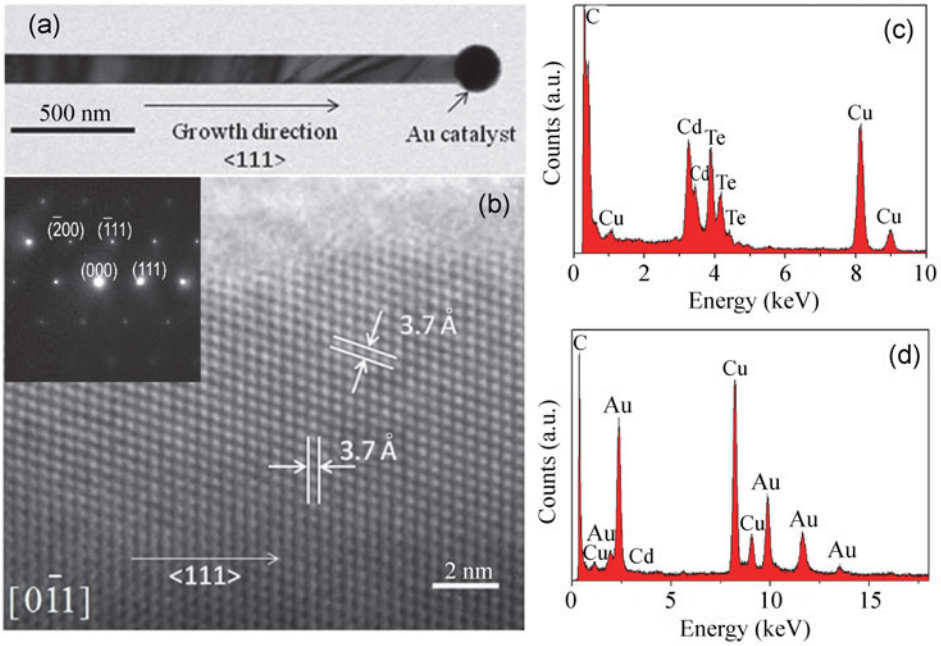

Figure 2 (a) Low magnification TEM image of a CdTe nanowire showing a nanoparticle on the tip of the nanowire. (b) HRTEM image shows the growth direction along <111>. Insert: SAED pattern of the HRTEM image. (c) EDS spectrum of CdTe nanowires. (d) EDS spectrum of the Au nanoparticle on the tip CdTe nanowires.

along <111>. Figures 2(c) and 2(d) show the local EDS spectra of the nanowire and the Au catalytic nanoparticle, respectively, in which the C and Cu peaks originated from the carbon-coated copper TEM grid. The EDS spectrum of the nanowire shows distinct cadmium (Cd) and tellurium (Te) peaks, and the atomic ratio of Cd:Te is calculated to be ~1:1, suggesting the material is close to stoichiometric. The EDS spectrum of the nanoparticle indicates the composition is primarily Au (~92 at.%) with a small amount of Cd (~8 at.%), and the Te content is below the detection limit. According to the Au–Cd phase diagram, at the low growth temperature employed (350 ˚C), the Au–Cd alloy is in solid form. Thus, the growth of CdTe nanowires is governed by a VSS growth mechanism. From the high resolution SEM image (insert of Fig. 1), the Au catalyst shows a polygonal shape after growth, which is a further evidence of VSS growth.

We should point out that these nanowires grow via a hydrogen-assisted VSS process, where hydrogen plays an important role. The formation is detailed as follows: First, the CdTe source reacts with H_2 gas, forming Cd and H_2Te vapors; subsequently, H_2Te decomposes into H_2 and Te_2 vapor. The process is known as hydrogen-assisted thermal evaporation [10, 11]. The reactions are expressed as

$$CdTe(s) + H_2(g) \longrightarrow Cd(g) + H_2Te(g)$$

$$H_2Te(g) \longrightarrow H_2(g) + 1/2Te_2(g)$$

The vapors are transported downstream in the furnace to the region where the Au-coated Si substrate is placed. Cd, Te, and H_2Te vapors then diffuse on the surface or inside the Au catalyst clusters, forming CdTe following the reaction

$$2Cd + H_2Te + 1/2Te_2 \longrightarrow 2CdTe(s) + H_2(g)$$

As excess source atoms are present, CdTe crystallizes at the catalyst/semiconductor interface since it is energetically favourable, resulting in nanowire growth. The hydrogen-assisted growth mechanism is verified by the fact that very few CdTe nanowires are grown in pure Ar gas, in contrast to the high density CdTe nanowires obtained in H_2. This suggests that the dissociation of CdTe source is suppressed in Ar. This is as expected, since Cd and Te form strong covalent bond with a bond energy of ~1.1 eV, and the

thermal energy (at 465 °C) alone is not sufficient to break the bond.

Residual strain commonly exists in nanowires grown on a substrate with thermal expansion coefficient and lattice mismatch [12, 13]. A lattice mismatch-induced strain field is usually found to concentrate around the base of the nanowires [12]. In addition, surface relaxation and reconstruction [14, 15], impurities (such as Au) and defects (such as point defects, stacking faults, and dislocations) generate lattice distortion [16], which can all contribute to residual strain in the nanowires. We focus here on the strain effects in the CdTe nanowires through a systematic investigation of the structural and optical properties of the nanowires. Figure 3 shows the XRD $\theta/2\theta$ scan pattern of the CdTe nanowire. The diffraction peaks (2θ) at 24.0°, 39.5°, 46.7°, 57.0°, 62.7°, 71.5°, and 76.4° are respectively indexed to (111), (220), (311), (400), (331), (422), and (511) diffraction peaks of the zinc blende structure of CdTe. The peaks of the unstrained zinc blende structured CdTe are located at 23.800°, 39.356°, 46.514°, 56.877°, 62.523°, 71.358°, and 76.431°, respectively (JCPDS card No. 65-8879). All the peaks are broadened and shifted, suggesting the presence of residual strain in the nanowires. A small fraction of wurtzite CdTe phase (< 2%) (JCPDS card No. 19-0193) can also be identified, originating from stacking faults in some nanowires. Strain along the nanowire axis (i.e., the <111> direction) is determined from the XRD (111) peak. The (111) peak has a FWHM of 0.418°, which is much broader compared to the peak width that would be induced by size confinement. This originates in fact from the inhomogeneous stress distribution in the CdTe nanowires. The lattice constant calculated from the (111) peak is a = 0.6417 ± 0.0056 nm and the lattice constant for unstrained CdTe is a_0 = 0.6482 nm [17], so that the compressive strain along the nanowire axis is determined to be $\varepsilon_{//} = (a - a_0)/a_0 = (-1.0 \pm 0.9) \times 10^{-2}$. (Note that the subscripts // and ⊥ are used to denote strain components parallel or perpendicular to the nanowire axis). Similarly, the strain component in the plane perpendicular to the nanowire axis is calculated to be $\varepsilon_{\perp} = (+0.4 \pm 1.0) \times 10^{-2}$ from the (220) diffraction peak. Since strain alters the band structure of the nanowires [14], they affect the optical properties of the nanowires.

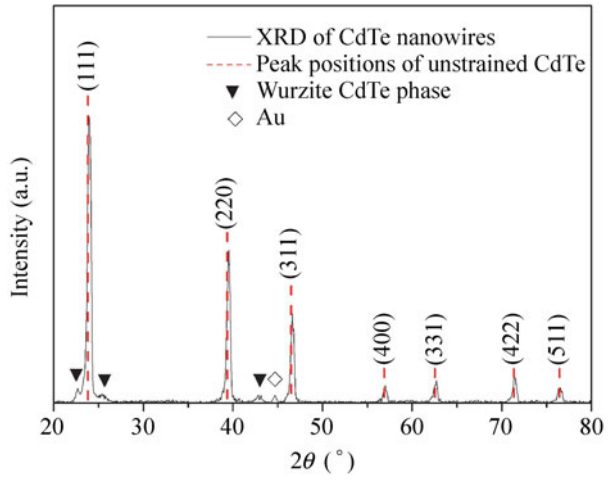

Figure 3 XRD pattern of CdTe nanowires. Miller indices of the zinc blende CdTe peak are indicated. The p eaks labelled by triangles originate from wurtzite CdTe, and the peak denoted with a diamond originates from the Au catalytic particle.

To verify the strain effect, the low temperature PL spectrum was measured at 5.0 K (Fig. 4(a)). It is dominated by a peak around 1.552 eV, with a small shoulder at 1.598 eV (peak 1 as noted in Fig. 4(a)), and two broad bands centred at 1.494 eV (peak 4) and 1.335 eV (peak 5). The PL spectrum was Gaussian fitted, as shown in Fig. 4(a), with fitted peaks delineated by the dashed lines. Note that the Gaussian fit yields two emission peaks at 1.552 and 1.553 eV (labelled as peaks 2 and 3). The origins of the peaks are designated according to the PL peak position of zinc blende CdTe taken from the Refs. [18–22]. The corresponding band diagram is shown in Fig. 4(b), illustrating the different observed transitions. Note that the PL spectrum is expected to arise predominantly from zinc blende CdTe, since the XRD pattern in Fig. 3 indicates the wurtzite content is less than 2%. The peak at 1.598 eV (peak 1) originates from the emission of donor bound excitons [18]. The bound exciton emission peak is weak because of enhanced surface recombination. The peak centred around 1.55 eV is actually a double peak (peaks 2 and 3) consisting of a donor–acceptor-pair (DAP) transition channel and a free electron to acceptor (e,A) transition channel related to the same acceptor energy level [19–21]. The corresponding acceptor state is located at ~50 meV above the valence band edge, and is likely to originate from the defect

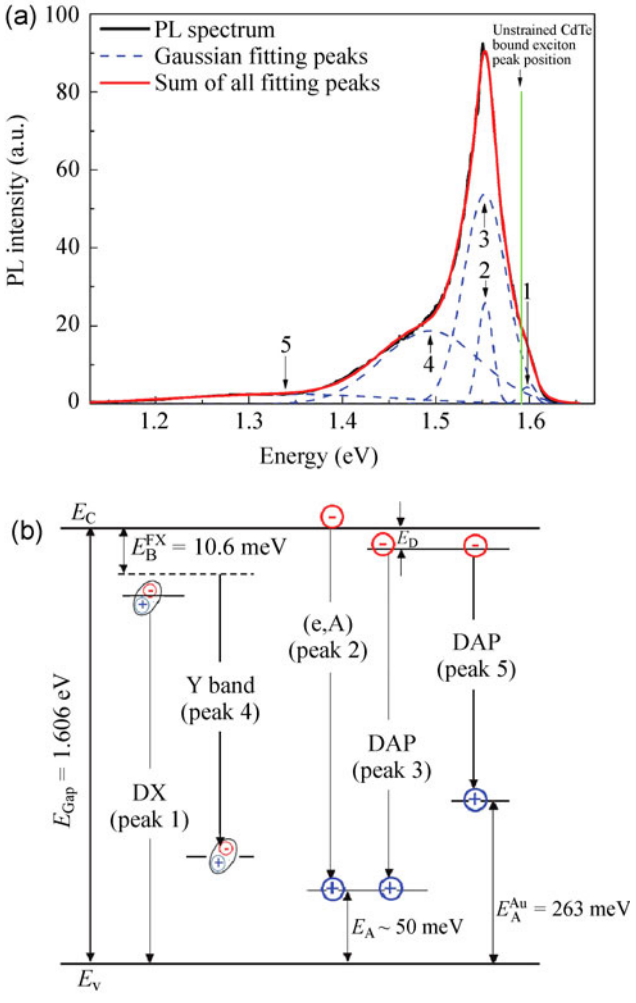

Figure 4 (a) Photoluminescence spectrum of CdTe nanowires measured at 5.0 K. A pronounced blue-shift in the bound exciton peak (peak #1) is observed. (b) The band structure for CdTe showing the transition processes: Donor bound excitons (DX), Y band, free electron to acceptor transitions (e, A), and donor–acceptor-pair transition (DAP) originating from shallow acceptors and deep level Au acceptors.

state due to Cd vacancies (V-Cd) or defect complexes involving V-Cd [18]. Note that double peaks have previously been reported to be in the range of 1.550 to 1.559 eV, varying with sample preparation [19–21]. The 1.494 eV peak can be identified as the well-known Y luminescence band, originating from the excitons bound to the structural dislocations, whilst the peak at 1.335 eV can be attributed to a DAP transition involving Au acceptors (with energy level E_{Au} about 263 meV above the valence band) and an unidentified shallow donor located a few meV below the conduction band [22].

The designation of the peak origins are further verified by the temperature-dependent PL measurements, as shown in Fig. 5. All the PL spectra were Gaussian fitted and the integrated PL intensity of each peak as a function of temperature is shown in the insert. The integrated PL intensity of peak 1 decreases as temperature rises from 5.0 to 20.0 K, and cannot be reliably distinguished in curve fitting for measurements at or above 34.6 K. This is consistent with the temperature dependence of bound exciton emission due to the delocalization and dissociation of bound excitons at increased temperature. In addition, the integrated PL intensity of the double peaks (2 and 3) shows distinct temperature-dependent behavior. The 1.552 eV peak (peak 3) shows a pronounced decrease as temperature increases from 5.0 to 20.0 K, while in contrast, the integrated PL intensity of the 1.553 eV (peak 2) peak shows only a slight decrease. Differences in temperature dependence of the integrated PL intensity are key characteristics distinguishing DAP transitions and (e,A) type transitions. With increase in temperature, shallow donors ionize, resulting in a suppression of the DAP transition. Consequently, the integrated PL intensity of a DAP transition peak decreases faster than that of an (e,A) type transition. As the temperature further increases to 34.6 K, more donor ionize, leading to the diminution

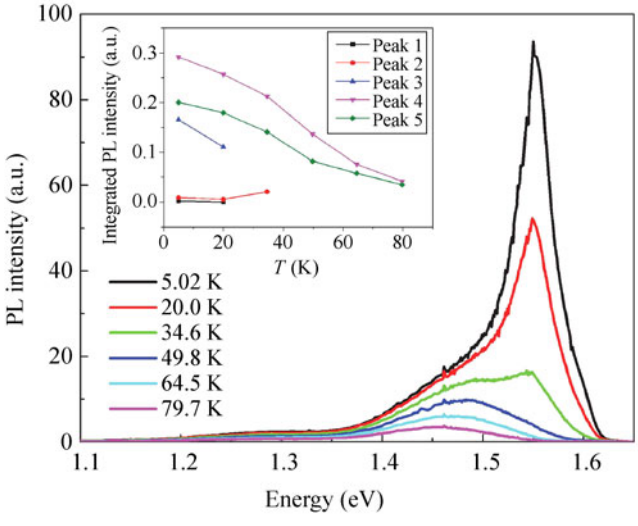

Figure 5 Temperature-dependent photoluminescence spectra of CdTe nanowires from 5.0 to 79.7 K. Insert: Temperature dependence of the integrated peak intensity for all five Gaussian fitted peaks (see Fig. 4 for peak assignment).

of the DAP peak (peak 3) and an increase in intensity of the (e,A) peak (peak 2). Therefore, the 1.552 eV peak (peak 3) originates from the DAP transition, and the 1.553 eV peak (peak 2) can be attributed to (e,A) type transition.

The temperature dependence of the Y luminescence band has been studied in relation to the recombination kinetics. Y luminescence is caused by the radiative decay of dislocation bound excitons, and thus the recombination processes involves the capture of free excitons to the dislocation sites and the thermal release of excitons from dislocations [23]. Thus, the temperature dependence of the integrated Y luminescence intensity can be derived by carefully balancing these two processes, and the activation energy for the thermal quenching process can be determined. Following Ref. [23], the temperature dependence of the Y band (peak 4) can be fitted with expression

$$I_{\mathrm{Y}} = \frac{I_0}{1 + \alpha T^{2/3} \exp(-E_{\mathrm{B}} / k_{\mathrm{B}} T)}$$

where I_{Y} is the integrated intensity of the Y band peak, I_0 and α are temperature-independent parameters, k_{B} is the Boltzmann constant and E_{B} is the binding energy of the exciton to the structural dislocations. The term $T^{2/3}$ comes from the effective density of exciton states, which is usually neglected in a simple theoretical model. E_{B} is fitted to be 9.8 meV, consistent with the previous reported value for thin film CdTe samples [24].

The thermal quenching of the integrated PL intensity of peak 5 cannot be fitted with a single activation channel. Rather, it fits well with the experiment data by assuming the presence of two thermal activation channels for dissociating the electron–hole pairs. The integrated intensity can be formulated by the expression [24, 25]

$$I = \frac{I_0}{1 + \alpha_1 \exp(-E_1 / k_{\mathrm{B}} T) + \alpha_2 \exp(-E_2 / k_{\mathrm{B}} T)}$$

where I_0 is the zero temperature integrated intensity of the DAP peak, α_1 and α_2 are temperature-independent fitting parameters and E_1 and E_2 correspond to the activation energies for the two different thermal processes resulting in the non-radiative recombination. The fitting results yield E_1 = 4.76 meV and E_2 = 20.6 meV. To elucidate the actual physical channels for these two thermal processes, further theoretical investigation is needed.

Taking a closer look at the PL spectra, it is evident that the fitted PL peaks 1, 2, 3, corresponding to bound exciton, DAP, and (e,A) transitions, are broadened and shifted compared to those measured in high quality bulk CdTe crystals [18]. Evidently, the observed blue-shift and broadening of PL peaks cannot be a consequence of confinement effects in the nanowires (estimated to be less than 0.5 meV for these CdTe nanowires with diameters 50–200 nm, which are far greater than the CdTe exciton diameter of 15 nm). To rule out heating effects, power-dependent PL measurements were performed (as shown in Fig. S1 in the Electronic Supplementary Material (ESM)). If there are heating effects, the rise of nanowire temperature will result in a obvious red-shift of all PL peaks with increase in excitation power density. However, there is no observable red-shift in any of the peaks (as shown in Fig. S2 in the ESM), indicating a lack of heating. In addition, the XRD measured strain in the nanowire ensembles provides a hint of the origin of the blue-shift and broadening of PL peaks, which we can thus attribute to residue strain in the nanowires. It is worth noting that broadening of PL peaks (corresponding to strain distribution) does not necessarily occur for a single nanowire, but could potentially arise from different amounts of strain existing in different nanowires of various sizes in the ensemble.

In order to estimate how large an energy shift the strain field causes, we apply deformation potential theory [26]. Following the aforementioned XRD results, the magnitudes of the strain and its distribution along the nanowire axis and in-plane perpendicular to the axis are $\varepsilon_{//} = (-1.0 \pm 0.9) \times 10^{-2}$ and $\varepsilon_{\perp} = (+0.4 \pm 1.0) \times 10^{-2}$. As expected, the mean axial stress (-1.0×10^{-2}) and the mean in-plane stress (0.4×10^{-2}) measured are consistent with the Poisson effect and a Poisson ratio of ~0.41 for CdTe. The strain induced fractional volume change $\Delta V / V = \varepsilon_{//} + \varepsilon_{\perp}$ can be extracted using a lower-bound estimate by adding the maximum axial strain to the minimum transverse strain, and vice versa. This indicates that the distribution of the inhomogeneous strain induced fractional volume

change in the samples is greater than the range of – 0.66% to – 2.94%. As the strain induced energy shift roughly follows $\Delta E_g = (a_c - a_v)\Delta V / V$ where a_c and a_v are the conduction band and valence band deformation potentials [26], the distribution of ΔE_g corresponding to the inhomogeneous strain distribution in the samples is greater than the range of + 3 to + 13 meV. In other words, the exciton, shallow donor and acceptor related transition peaks are broadened by at least 10 meV as a result of the inhomogeneous distribution of the residual strain. This qualitatively explains the satisfactory Gaussian fitting of the bound exciton peak of the nanowire samples (peak 1 centred at ~1.598 eV at 5.0 K) and a peak with FWHM ~16 meV, in contrast to the reported bound exciton peak for high quality bulk crystalline CdTe samples (1.592 eV with ~1 meV FWHM) [18].

In summary, zinc blende single crystalline CdTe nanowires have been successfully synthesized by CVD. The nanowire growth is governed by a Au catalytic VSS mechanism. We find that hydrogen gas plays an important role in the growth of CdTe nanowires, serving not only as a carrier gas, but also as a reaction intermediate assisting thermal evaporation of CdTe sources. The flow rate of hydrogen gas must be adjusted in order to obtain single crystalline CdTe nanowires. We have shown by XRD that our CVD-grown CdTe nanowires have residual strains which alter the electronic band structure. The shift and broadening of the exciton and impurity energy levels have been clearly demonstrated by the temperature-dependent photoluminescence results. These studies show that the strain effects in nanowires need to be carefully considered in the interpretation of the optical and electrical behavior of nanomaterials and in the design of future nanoscale optoelectronic devices.

Acknowledgements

The syntheses, XRD, electron microscopy analysis and PL measurement were supported as a part of the Center for Energy Nanoscience funded by the U.S. Department of Energy, Office of Science, Energy Frontier Research Center (EFRC) program under Award Number DE-SC0001013. The authors thank G. J. Möthrath for technical assistance in this project.

Electronic Supplementary Material: Supplementary material (power-dependent PL measurements of excitation energy density varying from 0.014 W/cm^2 to 9.725 W/cm^2) is available in the online version of this article at http://dx.doi.org/10.1007/s12274-013-0390-y.

References

[1] Xu, D. S.; Chen, D.; Xu, Y. J.; Shi, X. S.; Guo, G. L.; Gui, L. L.; Tang, Y. Q. Preparation of II-VI group semiconductor nanowire arrays by dc electrochemical deposition in porous aluminum oxide templates. *Pure Appl. Chem.* **2000**, *72*, 127–135.

[2] Wang, F. D.; Dong, A.; Sun, J.; Tang, R.; Yu, H.; Buhro, W. E. Solution-liquid-solid growth of semiconductor nanowires. *Inorg. Chem.* **2006**, *45*, 7511–7521.

[3] Tang, Z. Q.; Kotov, N. A.; Giersig, M. Spontaneous organization of single CdTe nanoparticles into luminescent nanowires. *Science* **2002**, *297*, 237–240.

[4] Yang, Q.; Tang, K.; Wang, C.; Qian, Y.; Zhang, S. Y. PVA-assisted synthesis and characterization of CdSe and CdTe nanowires. *J. Phys. Chem. B* **2002**, *106*, 9227–9230.

[5] Yong, S. M.; Muralidharan, P.; Jo, S. H.; Kim, D. K. One-step hydrothermal synthesis of CdTe nanowires with amorphous carbon sheaths. *Mater. Lett.* **2010**, *64*, 1551–1554.

[6] Hou, J. W.; Yang, X. C.; Lv, X.; Peng, D.; Huang, M.; Wang, Q. Y. One-step synthesis of CdTe branched nanowires and nanorod arrays. *Appl. Surf. Sci.* **2011**, *257*, 7684–7688.

[7] Ye, Y.; Dai, L.; Sun, T.; You, L. P.; Zhu, R.; Gao, J. Y.; Peng, R. M.; Yu, D. P.; Qin, G. G. High-quality CdTe nanowires: Synthesis, characterization, and application in photoresponse devices. *J. Appl. Phys.* **2010**, *108*, 044301.

[8] Hochbaum, A. I.; Fan, R.; He, R.; Yang, P. D. Controlled growth of Si nanowire arrays for device integration. *Nano Lett.* **2005**, *5*, 457–460.

[9] Wang, D.; Dai, H. J. Low-temperature synthesis of single-crystal germanium nanowires by chemical vapor deposition. *Angew. Chem. Int. Ed.* **2002**, *114*, 4977–4980.

[10] Utama, M. I. B.; Peng, Z.; Chen, R.; Peng, B.; Xu, X.; Dong, Y.; Wong, L. M.; Wang, S.; Sun, H.; Xiong, Q. H. Vertically aligned cadmium chalcogenide nanowire arrays on muscovite mica: A demonstration of epitaxial growth strategy. *Nano Lett.* **2011**, *11*, 3051–3057.

[11] Lovergine, N.; Prete, P.; Cola, A.; Mazzer, M.; Cannoletta, D.; Mancini, A. M. Hydrogen transport vapor phase epitaxy of CdTe on hybrid substrates for X-ray detector applications. *J. Electron. Mater.* **1999**, *28*, 695–699.

[12] Taraci, J. L.; Hÿtch, M. J.; Clement, T.; Peralta, P.;

McCartney, M. R.; Drucker, J.; Picraux, S. T. Strain mapping in nanowires. *Nanotechnology* **2005**, *16*, 2365–2371.

[13] Seo, H. W.; Bae, S. Y.; Park, J.; Yang, H.; Park, K. S.; Kim, S. Strained gallium nitride nanowires. *J. Chem. Phys*. **2002**, *116*, 9492–9499.

[14] Li, S.; Yang, G. W. Universal scaling of semiconductor nanowires bandgap. *Appl. Phys. Lett.*, **2009**, *95*, 073106.

[15] Sarkar, S.; Pal, S.; Sarkar, P. Electronic structure and band gap engineering of CdTe semiconductor nanowires. *J. Mater. Chem*. **2012**, *22*, 10716–10724.

[16] Shi, W. S.; Zheng, Y. F.; Wang, N.; Lee, C. S.; Lee, S. T. Oxide-assisted growth and optical characterization of gallium-arsenide nanowires. *Appl. Phys. Lett.* **2001**, *78*, 3304–3306.

[17] Ebina, A.; Takahashi, T. Studies of clean and adatom treated surfaces of II-VI compounds. *J. Cryst. Growth* **1982**, *59*, 51–64.

[18] Shin, H. Y.; Sun, C. Y. The exciton and edge emissions in CdTe crystals. *Mater. Sci. Eng. B* **1998**, *52*, 78–83.

[19] Aguilar-Hernández, J.; Cárdenas-García, M.; Contreras-Puente, G.; Vidal-Larramendi, J. Analysis of the 1.55 eV PL band of CdTe polycrystalline films. *Mater. Sci. Eng. B* **2003**, *102*, 203–206.

[20] Kraft, C.; Metzner, H.; Hädrich, M.; Reislöhner, U.; Schley, P.; Gobsch, G.; Goldhahn, R. Comprehensive photoluminescence study of chlorine activated polycrystalline cadmium telluride layers. *J. Appl. Phys.* **2010**, *108*, 124503.

[21] Van Gheluwe, J.; Versluys, J.; Poelman, D.; Clauws, P. Photoluminescence study of polycrystalline CdS/CdTe thin film solar cells. *Thin Solid Films* **2005**, *480–481*, 264–268.

[22] Molva, E.; Francou, J. M.; Pautrat, J. L.; Saminadayar, K.; Dang, L. S. Electrical and optical properties of Au in cadmium telluride. *J. Appl. Phys.* **1984**, *56*, 2241–2249.

[23] Hildebrandt, S.; Uniewski, H.; Schreiber, J.; Leipner, H. S. Localization of Y luminescence at glide dislocations in cadmium telluride. *J. Phys. III France* **1997**, *7*, 1505–1514.

[24] Halliday, D. P.; Potter, M. D. G.; Mullins, J. T.; Brinkman, A. W. Photoluminescence study of a bulk vapour grown CdTe crystal. *J. Cryst. Growth* **2000**, *220*, 30–38.

[25] Bimberg, D.; Sondergeld, M. Thermal dissociation of excitons bounds to neutral acceptors in high-purity GaAs. *Phys. Rev. B* **1971**, *4*, 3451–3455.

[26] Van de Walle, C. G. Band lineups and deformation potentials in the model-solid theory. *Phys. Rev. B* **1989**, *39*, 1871–1883.